Atmospheric Environment 193 (2018) 290–301

Contents lists available at ScienceDirect

Atmospheric Environment

journal homepage: www.elsevier.com/locate/atmosenv

Assessing air-quality in Beijing-Tianjin-Hebei region: The method and mixed tales of $PM_{2.5}$ and O_3

Lei Chen[a], Bin Guo[b,c,**], Jiasheng Huang[d], Jing He[c], Hengfang Wang[e], Shuyi Zhang[a], Song Xi Chen[a,f,*]

[a] Guanghua School of Management, Peking University, Beijing, 100871, China
[b] Center of Statistical Research, Southwestern University of Finance and Economics, Chengdu, 611130, China
[c] School of Statistics, Southwestern University of Finance and Economics, Chengdu, 611130, China
[d] School of Mathematical Science, Peking University, Beijing, 100871, China
[e] Department of Statistics, Iowa State University, Iowa 50010-1210, USA
[f] Center for Statistical Science, Peking University, Beijing, 100871, China

ARTICLE INFO

Keywords:
Air quality assessment
Meteorological confounding
Temporal adjustment

ABSTRACT

Motivated by a need to evaluate the effectiveness of a campaign to alleviate the notorious air pollution in China's Beijing-Tianjin-Hebei (BTH) region, we outline a temporal statistical adjustment method which is demonstrated from several aspects on its ability to remove the meteorological confounding existed in the air quality data. The adjustment makes the adjusted average concentration temporally comparable, and hence can be used to evaluate the effectiveness of the emission reduction strategies over time. By applying the method on four major pollutants from 73 air quality monitoring sites along with meteorological data, the adjusted averages indicate a substantial regional reduction from 2013 to 2016 in $PM_{2.5}$ by 27% and SO_2 by 51% benefited from the elimination of high energy consumption and high polluting equipments and a 20.7% decline of the coal consumption, while average NO_2 levels had been static with a mere 4.5% decline. Our study also reveals a significant increase in the ground O_3 by 11.3%. These suggests that future air quality management plans in BTH have to be based on dual targets of $PM_{2.5}$ and O_3.

1. Introduction

As China industrializes, chronic air pollution with excessive concentrations of pollutants are widely encountered in a substantial part of the country. The air pollution is known to cause serious health, social and economic issues. Epidemiological studies show that exposure to air pollution has significant adverse effects on human health (Pope et al., 2002; Baccarelli et al., 2014; Dominici et al., 2014; Rich et al., 2015; Guo et al., 2015). Chen et al. (2013) found a significant negative influence on life expectancy under sustained exposing to air pollution in China's Huai River area.

The Beijing-Tianjin-Hebei region is at the heart of the North China Plain and has experienced the severest air pollution in China. Cities in BTH ordinarily occupied more than half of the spots in the 10 most polluted cities in the country. There were in average 6.6 cities from BTH appeared among the 10 most polluted cities every month from 2013 to 2016. The underlying reason for the problem is excessive emission of pollutants from vast installations of heavy industries ranging from steel and iron making to building materials while assisted by increasing number of motor vehicles. At the same time, the dispersion condition of the region is not good as the BTH is surrounded by Taihang Mountain range on the west and Yan Mountain range at the north. This geography is ideal for fostering secondary generation of fine particulate matters $PM_{2.5}$.

To mitigate the notorious air pollution problem, China's State Council unveiled a “National Ten Point Plan” (China's State Council, 2013) in September 2013 that sets specific reduction targets in terms of annual $PM_{2.5}$ averages for various regions of the country by Year 2017. The reduction target for BTH region is “a 25% reduction over the Year 2012 level by Year 2017”, and that for Beijing is “no more than 60 $\mu g/m^3$”. There have been various strategies implemented by the authorities in BTH to tackle the air pollution problem. One is to curtail coal consumption by phasing out its use in power plants and in the winter heating with the natural gas in the 13 prefecture level or above

* Corresponding author. Guanghua School of Management, Peking University, Beijing, 100871, China.
** Corresponding author. Center of Statistical Research, Southwestern University of Finance and Economics, Chengdu, 611130, China.
E-mail addresses: csx@gsm.pku.edu.cn (S.X. Chen), guobin@swufe.edu.cn (B. Guo).

https://doi.org/10.1016/j.atmosenv.2018.08.047
Received 2 May 2018; Received in revised form 16 July 2018; Accepted 23 August 2018
Available online 30 August 2018

cities in BTH. The other is a tougher enforcement on the environmental laws and more strict crackdowns on excessive emissions by factories.

As the observed air pollution is ordinarily impacted by the meteorological condition (Wang et al., 2014; Liang et al., 2015; Tao et al., 2016), a decrease in observed concentrations may be either due to a decrease in emission or due to a favorable meteorological condition for the dispersion of pollutants. The latter is the so-called meteorological confounding. In order to measure the underlying temporal change in the pollution concentrations, we need to compare the air quality data of different years on a common temporal meteorological baseline. As demonstrated in this paper, re-calculating the concentrations on the meteorological baseline makes air quality statistics (averages and quantiles) comparable over the years, and hence removes the confounding.

Studies on the air quality of a city or region are generally based on air quality monitoring data obtained from monitoring sites and/or satellite remote sensing data. Air quality assessments based on data from a small number of monitoring sites per city was carried out in China's air pollution studies in recent years. These include Liang et al. (2015) that evaluated Beijing's air quality from Year 2010 to 2014 using the US Embassy's $PM_{2.5}$ data; and Liang et al. (2016) that analyzed $PM_{2.5}$ observations from the national pollutant monitoring stations. Also, much attention has been paid to the composition of the pollutants (Wang et al., 2007; Yang et al., 2011; Liu et al., 2016) and impacts of meteorological variables. Geographical condition is another important factor that affects the pollutant's concentrations and diffusion. By analyzing the $PM_{2.5}$, aerosol optical depth (AOD), and long-term visibility data, along with various climate and meteorological factors and the boundary layer structure, Wang et al. (2014) found that the unfavorable geographical condition of BTH region limited the diffusion of pollutants. In addition, Wang et al. (2014) showed an evidence that high humidity contributed to the aerosols and secondary transformation under high emission, leading to severe $PM_{2.5}$ episodes in Beijing in January 2013. There also have been studies by analyzing aerosol optical depth (AOD) data from satellite remote sensing. The focus there was to calibrate the ground-level $PM_{2.5}$ concentrations from the AOD (Martin, 2008; Wang et al., 2010; Geng et al., 2015; Van Donkelaar et al., 2015). This approach provides a well coverage for areas where ground monitoring sites are not available. Although the calibrated $PM_{2.5}$ from the AOD data provide a broad spatial-temporal coverage, they are subject to relatively large calibration errors, which depend on meteorological factors and the model used in the calibration (Liu et al., 2009; Chen et al., 2017).

This current study has two purposes. One is to demonstrate the need and effects of the meteorological adjustment for air quality assessment. The other is to conduct air quality assessment over BTH based on data with much more monitoring sites and meteorological information than previous studies. The latter is designed to provide a comprehensive assessment on the concentrations of four air pollutants: $PM_{2.5}$, sulfur dioxide (SO_2), nitrogen dioxide (NO_2), and the ground ozone (O_3) for 18 consecutive seasons between spring of Year 2013 and summer of 2017 in the 13 major cities in BTH.

Our study finds significant declines in $PM_{2.5}$ and SO_2 in the region. It also reveals a significant increase in the ground ozone level at a quite alarming rate, and a static nitrogen dioxide concentration. These indicate the air quality management in BTH should be transformed from a sole target of $PM_{2.5}$ to a new system with dual targets of $PM_{2.5}$ and O_3. This new dual targets' system should have the list of the primary precursors extended to include NO_x and volatile organic compounds in addition to SO_2, which demands a new strategy in this next phase of air quality management for BTH.

2. Data

2.1. Air quality data

China established a national air quality monitoring network in January 2013 that provides hourly recordings on six common air pollutants. Our analysis on BTH is based on hourly concentrations of the $PM_{2.5}$, SO_2, NO_2 and the ground ozone O_3 from 73 "Guokong" monitoring sites in BTH with Beijing and Tianjin each having 11 monitoring sites, and the remaining 51 sites from the 11 prefecture level cities in Hebei province. "Guokong" means sites are directly managed by the Ministry of Environment and Protection (MEP) in data collection with instantaneous transmission to a data centre in Beijing to avoid any potential local interference. Fig. S1 in the supplementary materials (SM) displays the locations of the 73 air quality monitoring sites as well as the 13 cities in the study region.

The first two months of Year 2013 saw the air quality data had high proportions of missing values, which led us to consider data from March 2013 until August 2017. The time unit of our assessment is season such as spring from March to May, summer June to August, fall September to November, and winter December to February next year. This comes from a consideration that a season in BTH offers quite homogeneous weather conditions and sufficient amount of data for the meteorological adjustment. As a result, we use the seasonal year from March to February next year rather than the calendar year.

2.2. Meteorological data

As the observed pollutants' concentrations are ordinarily impacted by the meteorological condition, we employ meteorological data at 21 weather observing stations from China Meteorological Administration (CMA) in the 13 cities. Among the 21 weather stations, 11 were from the 11 prefecture level cities in Hebei with each city having one station, 7 from Beijing and 3 from Tianjin. Table S1 shows the matching between air quality monitoring sites and the corresponding meteorological stations. The meteorological data consists of six hourly variables: *air pressure (PRES), temperature (TEMP), dew point (DEWP), wind direction (W), cumulative wind velocity (CWS) and cumulative precipitation (R)*. The wind directions on the rose wind plot are grouped into five categories $\Omega = \{NW, NE, SW, SE, CV\}$ *with* $NW = (W,N,NW,NNW,WNW)$, $NE = (NE,NNE,ENE)$, $SW = (SW,SSW,WSW)$, $SE = (E,S,SE,ESE,SSE)$ and *CV* contains both the calm and variable wind as well as the wind whose speed is less than 0.5m/s. The cumulative wind velocity is defined as summation of the wind velocity since the hour that a wind direction was established. The definition of the cumulative precipitation is similar by adding up hourly precipitation amount over consecutive hours with non-zero precipitation. Any of these two variables is reset to zero whenever there is a change of wind direction or an hour without precipitation.

For ground ozone, solar radiation is a significant meteorological factor that influences its generation. We use the ultraviolet radiation with wavelengths between 200 and 440 nm, which is termed as UVB by the European Centre for Medium-Range Weather Forecasts (ECMWF). The UVB data are provided at a grid size of $0.25° \times 0.25°$ at hourly frequency available over the study region.

The process of O_3 generation triggered by the solar radiation has a delayed effect, which is reflected by the time series of O_3 being lagged behind that of the UVB as shown in Fig. S2 of the SM. We calculate the correlation between O_3 and the cumulative lagged UVBs ranging from 0 to 11 h. Our analysis shows that the maximum correlation between the ozone concentration within the 8 h between 12:00 and 19:00 and the cumulative lagged UVBs was attained at lag 7 in the spring, lag 6 in the summer and the fall, lag 4 for the winter. The detailed correlations are reported in Table S2 of the SM. Hence, we use these numbers of lagged cumulated UVB values and take a logarithm transform for the four seasons as a covariate in the adjustment for O_3.

The weather data are from March 2010 to August 2017, three years more than the timespan of air quality data. The latter is to allow the construction of a temporally meteorological baseline at each city for the meteorological adjustments.

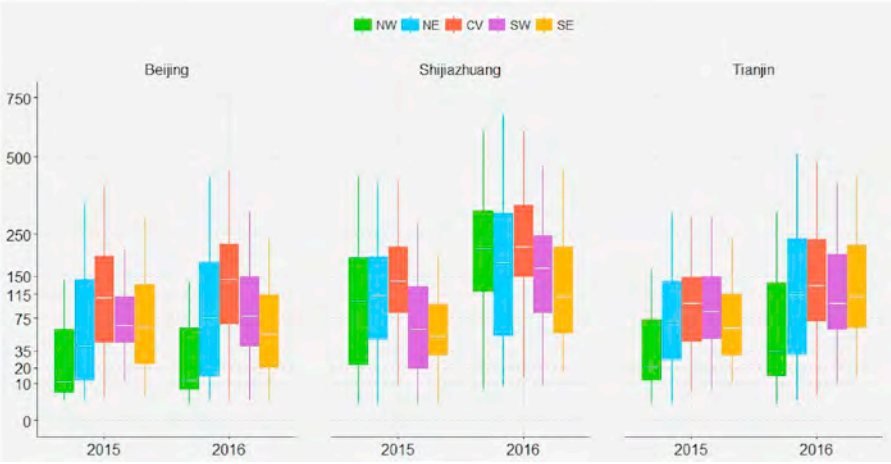

Fig. 1. Boxplots of $PM_{2.5}$ concentrations ($\mu g/m^3$) under five wind directions in Beijing Wanliu, Shijiazhuang Gaoxinqu and Tianjin Beichen sites in the winter of 2015 and 2016. The white lines are the medians.

3. Meteorological confounding

A common way to compare air quality between two time periods is to calculate the raw averages of a pollutant, say $PM_{2.5}$, from the hourly concentrations in the two periods. As the raw $PM_{2.5}$ concentrations are highly affected by the weather condition, these two averages are not comparable from the view point of gauging on the underlying pollution emission, as the weather conditions of the two periods are not the same.

To reveal the drawbacks of the approach, Fig. 1 displays the average concentrations of $PM_{2.5}$ under the five wind directions at Beijing Wanliu site, Shijiazhuang Gaoxinqu and Tianjin Beichen sites, in the winters of 2015 and 2016, respectively. It shows that $PM_{2.5}$ is highly dependent on the wind direction. The concentration is the lowest under NW for Beijing and Tianjin, and under SE for Shijiazhuang. The wind direction with low $PM_{2.5}$ corresponds to the direction of lower emission area of a city. The concentration is the highest under the CV for the three cities as CV is associated with static air that is strongly associated with severe pollution.

Fig. 2 displays the percentage compositions of the five wind directions and their average cumulative speed of Beijing Wanliu site in the winters of 2015, 2016 and a baseline constructed from seven winters' data from 2010 to 2016. Table 1 provides numerical values of the average $PM_{2.5}$ under the five wind directions and their percentages corresponding to Fig. 2. It is obviously that the wind percentages varied substantially each year. For instance, the winter of 2016 has around 9% less NW wind than that of the 2015 and the baseline, and also has much weaker wind speed of NW. The percentage of CV in 2016 is 4% more than the baseline, and 2.5% more than 2015's. This lower NW and higher CV for 2016 mean that the pollution level in the winter of 2016 would be higher than that of the 2015.

Indeed, according to Table 1, the raw average in the winter 2016 in Beijing is 105.7 $\mu g/m^3$, 21.6% more than the winter 2015's average of 86.9 $\mu g/m^3$. However, this 21.6% exaggerated the increase of the underlying emission as part of the increase is due to the winter 2016 having less NW and more CV winds. This shows a confounding of the observed $PM_{2.5}$ by wind. The confounding makes the two raw averages not comparable as far as in reflecting the underlying emission.

A fairer comparison that is designed to measure the underlying emission level is to compute the potential average for winter 2016 under the 2015's wind composition, which is

$$\hat{\mu}_{2015}(2016) = \sum_{w\in\Omega} r_w(2015)\cdot\hat{\mu}_w(2016) = 98.0\mu g/m^3$$

where Ω is the set of the five wind directions, and $r_w(2015)$ denotes the 2015's percentage of a wind direction $w \in \Omega$, and $\hat{\mu}_w(2016)$ is the average concentration in winter 2016 for direction w. In statistical causal inference, $\hat{\mu}_{2015}(2016)$ is called a counter-factual or potential average (Morgan and Winship, 2014).

Similarly, the potential average of winter 2015 based on winter 2016's wind composition is

$$\hat{\mu}_{2016}(2015) = \sum_{w\in\Omega} r_w(2016)\cdot\hat{\mu}_w(2015) = 92.9\mu g/m^3$$

which is comparable with the raw 2016's average of 105.7 $\mu g/m^3$ as both are based on 2016's wind composition. Thus, the raw 2015's average of 86.9 $\mu g/m^3$ is comparable with $\hat{\mu}_{2015}(2016) = 98.0\mu g/m^3$ as both use 2015's wind as the basis.

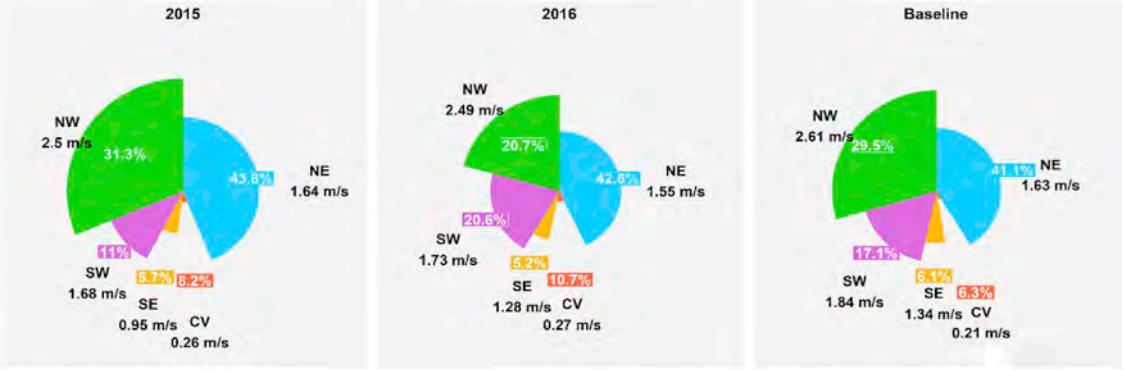

Fig. 2. A comparison of 5 wind directions occupying percentages in the winters of Beijing 2015, 2016 and baseline and the average wind speed. The baseline is the average level of 7 years from 2010 to 2016. The radius of the each fan-shaped area represent the average wind speed of the wind in the season.

Table 1
Wind composition statistics and the corresponding raw average $PM_{2.5}$ concentrations ($\mu g/m^3$) at Beijing Wanliu monitoring site in the winters of 2015 and 2016 together with adjusted averages with respect to the baseline wind composition, the dew point and the full meteorological variables. The adjusted method is in section 4. The last line is the different kinds of seasonal averages. Values under the raw composition is the raw average concentration under the corresponding year wind composition. And the values under the adjusted block are under the baseline wind composition.

Wind Direction	2015 Winter					2016 Winter				
	Raw		Adjusted			Raw		Adjusted		
	Average	Composition	baseline	Dew point	Full	Average	Composition	baseline	Dew point	Full
NW	65.3	31.3%	29.4%	55.9	62.5	58.4	20.7%	29.4%	49.2	54.9
NE	89.8	43.9%	41.1%	86.8	95.3	112.0	42.9%	41.1%	93.4	106.5
CV	123.4	8.2%	6.3%	113.1	115.4	163.2	10.7%	6.3%	139.9	154.9
SW	106.7	10.9%	17.1%	119.6	100.3	116.9	20.5%	17.1%	109.0	123.1
SE	110.0	5.7%	6.1%	109.6	100.7	78.3	5.2%	6.1%	79.7	84.0
Average		86.9	88.8	86.3	88.0		105.7	98.2	85.1	95.8

From the view point of 2015's wind composition, the average $PM_{2.5}$ in 2016 increased by 11.1 $\mu g/m^3$ which is a 12.8% increase, while from the view of 2016's wind composition, the average in 2016 increase by 12.8 $\mu g/m^3$at 13.8%. Both are much milder than the 21.6% increase based on the raw averages. The extra percentages can be regarded as those contributed by the confounding.

When we compare pollution levels over several years, for instance 4 years in our current study, it is rather cumbersome to compute all pairs of potential averages. A simple approach is to adjust the averages over a temporal baseline wind composition that produces only one average per season per year. Mathematically, let $r_w(\cdot) = A^{-1}\sum_{a=1}^{A} r_w(a)$ be the average wind distribution based on A years' wind data. The right panel of Fig. 2 is one such $r_w(\cdot)$ based on $A = 7$ years' data from 2010 to 2016 (to 2017 for spring and summer). Then, average concentration pegged to the baseline $r_w(\cdot)$ for year a is

$$\hat{\mu}(a) = \sum_{w\in\Omega} r_w(\cdot)\cdot\hat{\mu}_w(a)$$

Table 1 provides the averages under the 7 years' baseline wind composition for the winters of 2015 and 2016 along with some other averages discussed above.

The observed $PM_{2.5}$ is not only confounded by wind, but also by other meteorological variables. Fig. 3 displays pair-wise contour plots of dew point, air pressure and temperature with super-imposed $PM_{2.5}$ concentration. The confounding of $PM_{2.5}$ by the dew point is the most visible, as low (high) $PM_{2.5}$ is highly associated with low (high) dew point. And yet, as shown in Panel (d) of Fig. 3, the distribution of the dew point (and the other two variables) varied substantially among the winters of 2015, 2016 and the baseline. This implies that $\hat{\mu}(a)$ is confounded by the dew point and other variables as it has only adjusted the wind composition.

4. Method

As shown in the previous section, in addition to the emission, the meteorological conditions also impact the pollutant's concentrations significantly. Indeed, a favorable meteorological condition with high emission can result in low $PM_{2.5}$ concentrations, while a static and stable weather can cause severe pollution even in a low emission regime. Therefore, instead of comparing raw concentrations, a statistical approach that can correct the meteorological confounding should be applied. Here, we consider a nonparametric model (Härdle, 1992) on

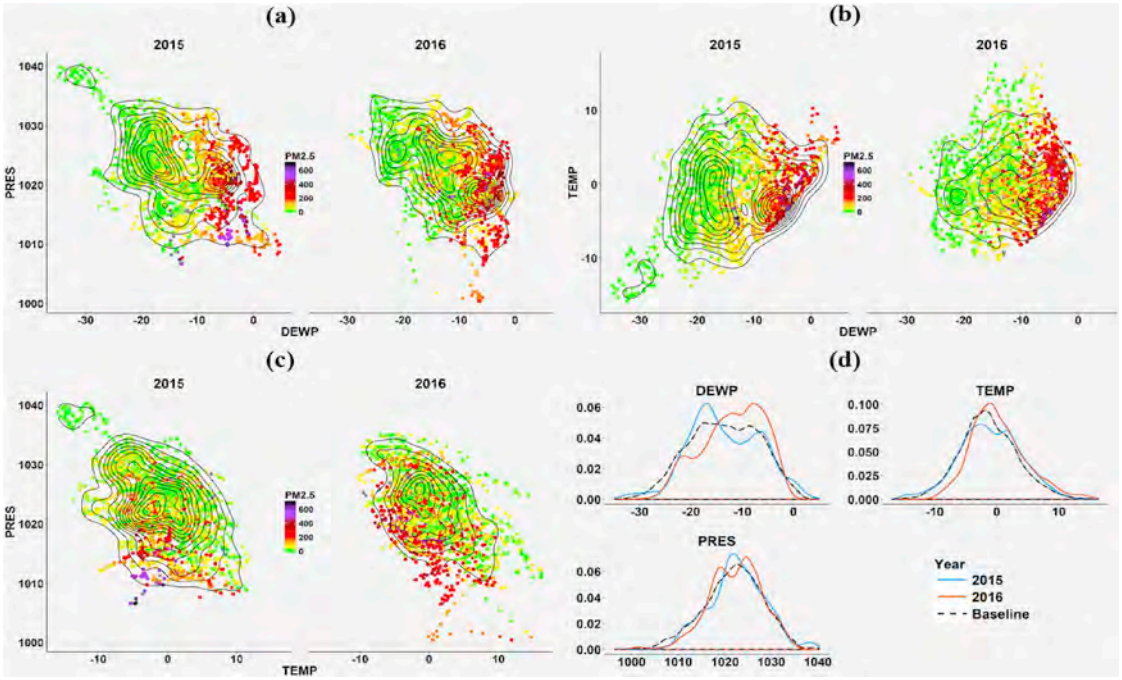

Fig. 3. The density of $PM_{2.5}$ concentration with respect to DEWP and PRES (a), DEWP and TEMP (b) and PRES and TEMP (c). Also, (d) shows the differences between 2015, 2016 and baseline of DEWP, TEMP and PRES.

the pollutant's concentrations, meteorological variables and emission.

4.1. Adjusted averages

In order to neutralize the meteorological effect, we consider a meteorological adjustment approach that was first proposed in Liang et al. (2015) and is refined and better presented here. The approach re-calculates the average concentrations of a pollutant under a temporally meteorological baseline condition based on the historical meteorological data which can remove the meteorological confounding. It consists of two key components. One is estimating the nonparametric regression function for the pollutant with respect to the meteorological variables, which not only include the wind composition, but also other related meteorological variables. The second component is to re-calculate the average on a temporal baseline meteorological condition based on longer weather records.

Let $Y_{ijt}(s)$ denote the concentration of a pollutant, say $PM_{2.5}$, at hour t in season j and year i of a monitoring site s, $W_{ijt}(s)$ represent the wind direction which is a discrete variable and $X_{ijt}(s)$ represent other meteorological variables, such as temperature ($TEMP$) and dew point ($DEWP$) etc. n_{ij} is the total number of observations in the season. We use the following model to quantify the relationship between pollutant concentrations and meteorological variables:

$$Y_{ijt}(s) = m_{ij}(X_{ijt}(s), W_{ijt}(s); s) + \varepsilon_{ijt}(s), \quad t = 1,2, \cdots, n_{ij} \tag{1}$$

where $\varepsilon_{ijt}(s)$ is the residual term. As the underlying emission is unobservable at the hourly frequency, it is not reflected in the model directly. However, it is implicitly embedded in the regression function $m_{ij}(\cdot)$. Also, part of the difference between $m_{i_1 j}(\cdot)$ and $m_{i_2 j}(\cdot)$ for two different years i_1 and i_2 is due to the difference of the underlying emission in the two years.

Next, we define a common probability baseline density function of the meteorological variables:

$$f_{.j}(x, w; s) = M^{-1} \sum_{a=1}^{M} f_{aj}(x, w; s) \tag{2}$$

where $f_{aj}(x, w; s)$ is the probability density function of the meteorological data (X, W) at season j of year a at site s, and M is the total number of years of available weather data. In our study, $M = 7$ or 8 as we use data from March 2010 to August 2017 to build the weather baseline while the air quality data were from March 2013 to August 2017.

The key in removing the meteorological confounding is to put the comparison under the same meteorological baseline $f_{.j}(x, w; s)$. Hence, we define the adjusted average concentration of year i at season j with respect to the baseline probability density $f_{.j}(x, w; s)$ as

$$\mu_{ij}(s) = \int m_{ij}(x, w; s) f_{.j}(x, w; s) dxdw \tag{3}$$

In contrast, by the law of large numbers, the raw average for season j of year a is actually the

$$\frac{1}{n_{aj}} \sum_{t=1}^{n_{aj}} Y_{ajt}(s) \xrightarrow{P} \eta_{aj}(s) = \int \int m_{aj}(x, \omega; s) f_{aj}(x, \omega; s) dxdw \tag{4}$$

where $\eta_{aj}(s)$ is calculated under the meteorological condition of year a only.

Suppose we want to measure the difference between the average pollution between years i and l. The one based on the adjusted averages in (3) is

$$\mu_{ij}(s) - \mu_{lj}(s) = \int (m_{ij}(x, w; s) - m_{lj}(x, w; s)) f_{.j}(x, w; s) dxdw$$

which is sole due to the change in the two regression functions $m_{ij}(x, w; s) - m_{lj}(x, w; s)$. However, for the one based on the un-adjusted version given in (4), it would be

$$\eta_{ij}(s) - \eta_{lj}(s) = \int (m_{ij}(x, w; s) f_{ij}(x, w; s) - m_{lj}(x, w; s) f_{lj}(x, w; s)) dxdw$$

which unfortunately cannot be attributed solely to the difference between $m_{ij}(x, w; s)$ and $m_{lj}(x, w; s)$ as it may be due to the different weather conditions expressed by $f_{ij}(x, w; s)$ and $f_{lj}(x, w; s)$ in the two years. Hence, $\eta_{ij}(s) - \eta_{lj}(s)$ is not suitable for an objective measure on the underlying emission.

To estimate the adjusted average concentration in (3), we firstly estimate the $m_{ij}(\cdot)$ function in (1) by using a nonparametric kernel regression estimator (Härdle, 1992; Fan and Yao, 2003):

$$\hat{m}_{ij}(x, w; s) = \frac{\sum_t \mathbf{K}_h(x - X_{ijt}(s)) I(W_{ijt}(s) = w) Y_{ijt}(s)}{\sum_u \mathbf{K}_h(x - X_{iju}(s)) I(W_{iju}(s) = w)} \tag{5}$$

where $I(\cdot)$ is the indicator function for wind direction. $\mathbf{K}_h(z) = k(z_1/h_1)k(z_2/h_2)\cdots k(z_5/h_5)/(h_1 h_2 \cdots h_5)$ is a multi-dimensional kernel function that is a product of the univariate Gaussian kernel $k(u) = (2\pi)^{-1/2}\exp(-u^2/2)$ with bandwidths $\{h_1, h_2, \cdots, h_5\}$. In practice, the bandwidths are chosen by the cross validation (CV) algorithm (Härdle, 1992; Chen and Tang, 2008).

Substituting $\hat{m}_{ij}(x, w; s)$ in Equation (5) to Equation (3), and replace baseline density $f_{.j}(x, w; s)$ with its empirical version, the adjusted average $\mu_{ij}(s)$ is estimated by

$$\hat{\mu}_{ij}(s) = \left(\sum_{a=1}^{M} n_{aj} \right)^{-1} \sum_{a=1}^{M} \sum_{t=1}^{n_{ij}} \sum_{w \in \Omega} \hat{m}_{ij}(X_{ajt}(s), W_{ajt}(s); s) I(W_{ajt}(s) = w) \tag{6}$$

To obtain the standard errors of the estimated adjusted average, the bootstrap re-sampling method is applied to generate repeated copies of the adjusted means as outlined in the SM.

The adjusted average concentration of a city is obtained by averaging the adjusted averages at all monitoring sites in the city, namely $\hat{\mu}_{ij} = S^{-1} \sum_{s=1}^{S} \hat{\mu}_{ij}(s)$, where S is the number of monitoring stations in the city. In addition to the adjusted average, adjusted 90% quantiles of the concentrations can be calculated for each city in a similar way which can measure the 10% most severe pollution concentration. The detailed composition together with the acquisition of its standard error are also given in the SM.

4.2. Adjusted curves

In this paper, we propose a new adjusted average function with respect to a meteorological variable, which we call the adjusted curve. This curve represents the relationship between a pollutant's average concentration and a meteorological variable after properly controlling the rest of meteorological variables. Often one wants to quantify the relationship between a pollutant's average concentration with respect to a meteorological variable, such as the dew point or air temperature. Directly regressing the pollutant data on the dew point without controlling the other meteorological variables will lead to confounded regression estimation. The baseline density function of the weather variables given in (2) can be used to produce the adjusted curves free of the confounding by the other variables.

Let $X^{(k)}$ be a meteorological variable that we would like to produce the adjusted curve, and $X^{(-k)}$ represent the rest of the meteorological variables. If $X^{(k)}$ is not the wind direction, the adjusted average curve with respect to $X^{(k)}$ can be defined as

$$\mu_{ij}(X^{(k)}; s) = \int \int m_{ij}(x^{(k)}, x^{(-k)}, w; s) f_{.j}(X^{(k)}, x^{(-k)}, w; s) dx^{(-k)} dw \tag{7}$$

where the integration is carried out without the $x^{(k)}$. If $X^{(k)} = W$ is a wind direction, then

$$\mu_{ij}(W; s) = \int m_{ij}(x, w; s) f_{.j}(x, W; s) dx \tag{8}$$

To estimate the adjusted curves, if $X^{(k)}$ is not the wind direction, one can estimate $\mu_{ij}(X^{(k)}; s)$ in (7) by

$$\hat{\mu}_{ij}(X^{(k)}; s) = \frac{1}{N(X^{(k)}, b)} \sum_{a=1}^{M} \sum_{X_{ajt} \in A(X^{(k)}, b)} \sum_{w \in \Omega} \hat{m}_{ij}(X_{ajt}, W_{ajt}; s) I(W_{ajt} = w) \tag{9}$$

where $A(X^{(k)}, b) = \{x = (\cdots, x^{(k)}, \cdots): X^{(k)} - b \le x^{(k)} \le X^{(k)} + b\}$ is a cross section of the X-domain which has its k-th component within a b neighborhood of $X^{(k)}$, $N(X^{(k)}, b)$ denotes the number of data that falls into $A(X^{(k)}, b)$, and $b > 0$ is a smoothing parameter that defines the size of the cross section.

If $X^{(k)} = W$, then

$$\hat{\mu}_{ij}(W; s) = \frac{1}{N(W)} \sum_{a=1}^{M} \sum_{t=1}^{n_{aj}} \hat{m}_{ij}(X_{ajt}, W_{ajt}; s) I(W_{ajt} = W) \tag{10}$$

where $N(W)$ denotes the number of data whose $W_{ajt} = W$. This is actually the adjusted average for a wind direction appeared in Table 1. The adjustment under a wind direction with respect either one or the rest of the meteorological variables can be defined similarly, and have already appeared in Table 1.

The adjusted average curves provide information on the pollutant's concentration with respect to the variable $X^{(k)}$, showing more details than the adjusted mean $\mu_{ij}(s)$ at (3). If one further integrate $X^{(k)}$ in (7) or (10) with respect to the marginal baseline probability density of $X^{(k)}$, $\mu_{ij}(s)$ will be reached.

Figs. 4 and 5 display the averaged raw curves and adjusted curves for $PM_{2.5}$ with respect to the dew point and the air temperature in the four winters from 2013 to 2016 over three air quality monitoring sites in Beijing and all six sites in Shijiazhuang. The three sites in Beijing and the six sites in Shijiazhuang shared a common meteorological station respectively, which we denote as Beijing M54399 and Shijiazhuang. The raw curves are simply the kernel regression estimation without adjusting for the other weather variables. These figures show that the raw curves are much less orderly and consistent over the years comparing with the adjusted ones. We find that by removing the confounding of the other variables, the adjusted curves have less curvature and become more consistent over the years. The latter curves for Beijing and Shijiazhuang show a clearer year separation which was especially the case for temperature.

Although the four yearly adjusted curves for the dew point is not as clearly separated as those curves for the temperature, by calculating the areas under the curves weighted by the baseline probability density function of the dew point, the overall adjusted averages are 91.6 for winter 2015, 94.2 and 96.4 for 2014 and 2013 respectively, and 104.0 for 2016, all in $\mu g/m^3$, which follow the same ordering as that of the temperature.

The raw and adjusted curves of 8-h (from 12pm to 7pm) O_3 with respect to the logarithm of the cumulated UVB for the summers are shown in Fig. 6. The adjusted curves are more monotone with respect to the logarithm of the cumulated UVB than the unadjusted ones. They also display a better separation with respect to the years, which is especially the case in Shijiazhuang. More comprehensive analysis on the adjusted 8-h O_3 will be made in Section 5.2.

4.3. Limitation of the moving average approach

Moving averages of certain number of years' (say 4–5 years') raw pollution concentrations have been advocated as a method to remove the meteorological confounding in China. We are to show that this approach can not remove the meteorological confounding, nor can it provide an adequate measure on the underlying changes by the air quality.

To make the argument concise, our discussion is confined to the underlying mathematical quantities without getting to empirical estimation. The same argument can be applied to the empirical version of the argument based on the law of large numbers and the notion of consistent estimations in statistics. Indeed, as shown in Equation (4), by the law of large numbers, the raw average concentration of season j in year i approximates

$$\eta_{ij}(s) = \int \int m_{ij}(x, \omega; s) f_{ij}(x, \omega; s) dx dw$$

As $\eta_{ij}(s)$ is averaged with respect to $f_{ij}(x, w; s)$, the probability density of year i and season j, it is ordinarily confounded by the weather condition of year i as revealed in Section 4.1. The moving average estimator based on M years' sample averages is

$$\bar{\eta}_{ij}(s) = M^{-1} \sum_{l=0}^{M-1} \eta_{(i-l)j}(s)$$

The problem with the moving average is that the yearly changes are equivalent to

$$\bar{\eta}_{ij}(s) - \bar{\eta}_{i-1j}(s) = M^{-1}\{\eta_{ij}(s) - \eta_{i-M+1j}(s)\}$$

which is actually the change in the (confounded) averages between year i and year $(i - M + 1)$, rather than anything on year i and year $(i - 1)$.

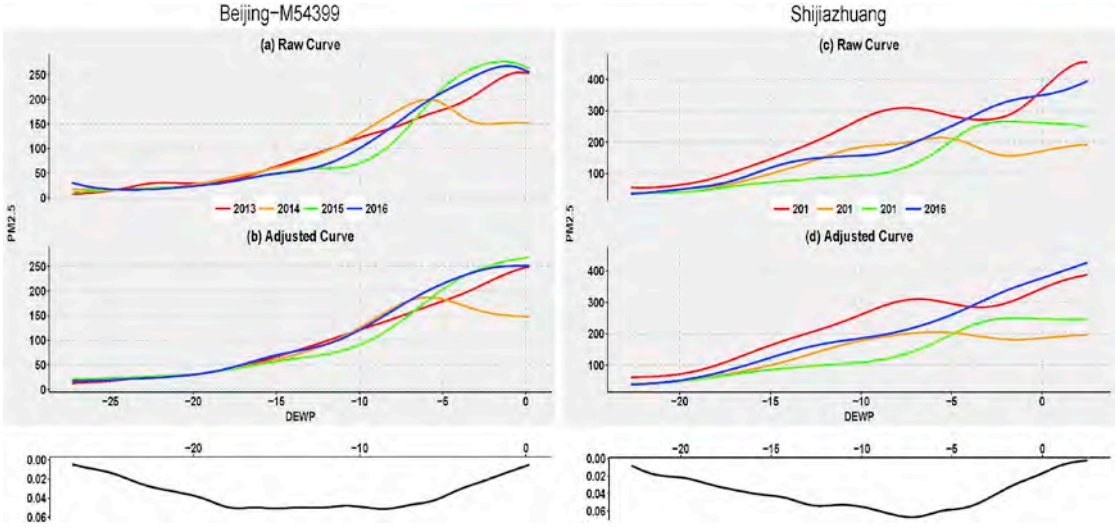

Fig. 4. Raw and Adjusted curves of $PM_{2.5}$ with respect to the dew point in winters from seasonal years 2013–2016 of Beijing-M54399 and Shijiazhuang. The curves of Beijing-M54399 denote the average over three air quality sites: Aotizhongxin, Guanyuan and Wanliu that share the same meteorological data from station 54399, while the curves of Shjiazhuang are averaged over six air quality sites that all shared the same weather data. The bottom curve under each plot is the baseline probability density of the dew point in each city.

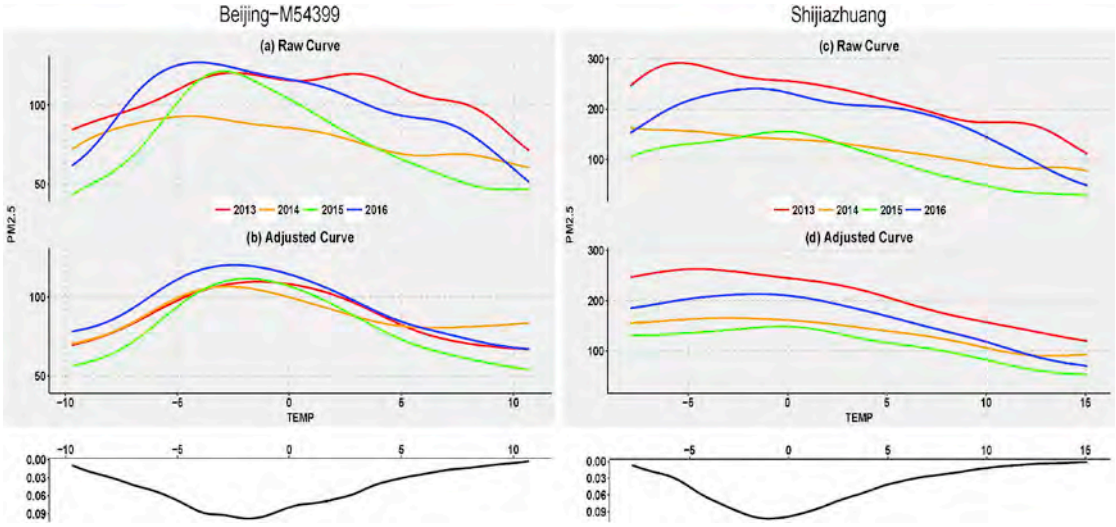

Fig. 5. Raw and Adjusted curves of $PM_{2.5}$ with respect to temperature in winters from seasonal years 2013–2016 of Beijing-M54399 and Shijiazhuang. The bottom curve under each plot is the baseline probability density of the temperature in each city. See caption of Fig. 4 for other specifics.

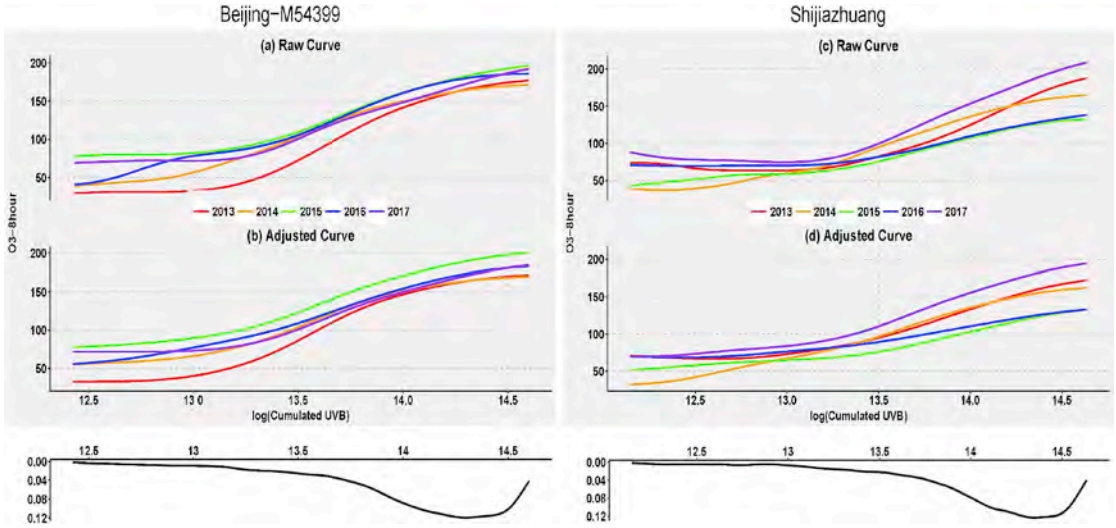

Fig. 6. Raw and Adjusted curves of 8-h O_3 with respect to logarithm of the cumulated UVB in summers from seasonal years 2013–2016 Beijing-M54399 and Shijiazhuang. The bottom curve under each plot is the baseline probability density of the logarithm of the cumulated UVB in each city. See caption of Fig. 4 for other specifics.

Also, all the pollution information in the middle years of the moving average has been canceled out. Hence, it is not suitable for objectively measuring the underlying change in the pollution level.

5. Air quality assessment for BTH region

To assess the air quality improvements of the BTH region since 2013, we apply the adjustment method to remove the meteorological confounding and calculate the meteorological adjustment concentrations for $PM_{2.5}$, SO_2, NO_2 and O_3 from spring 2013 to summer 2017. The results presented here are based on the adjusted average concentrations. The adjusted 90% quantiles of these four pollutants are presented in SM.

5.1. $PM_{2.5}$ and SO_2

$PM_{2.5}$ represents particulate matters (PM) with aerodynamic diameter less than 2.5 μm. It is one of the major urban air pollutants and can cause various harms to human health (Pope et al., 2002). In 2013, $PM_{2.5}$ replaced PM_{10} as the primary air pollutant in China, and has been a key target air pollutant in the "National Ten Point Plan". Sulfur dioxide (SO_2) is another major air pollutant which is not only harmful to human (Kampa and Castanas, 2008) but also a key gaseous precursor to $PM_{2.5}$ and PM_{10} (Baker and Scheff, 2007). As coal has been the main source of energy for industrial and domestic use in BTH and China at large, SO_2 is mainly the result of coal burning for power generation, winter heating, heavy industrial manufacturing for iron, steel and building materials.

Fig. 7 displays the seasonally adjusted averages of $PM_{2.5}$ and SO_2 for the 13 cities in the BTH from spring 2013 to summer 2017.

There are strong seasonality in the $PM_{2.5}$ and SO_2 concentrations with the winter having the highest level and summer the lowest in most of the cities in BTH. As shown in Fig. 7, the 13 cities in the BTH region can be grouped into three sub-regions as cities within the same sub-region share the similar seasonal variation pattern and concentration level. The grouping details are shown in Table 2.

The regionalization is highly correlated with the industrial layout in the BTH region. As for $PM_{2.5}$, its concentrations in the Northern sub-region were the lowest due to the sparse intensity of industrial establishment. In a sharp contrast, the five cities in the Along Taihang sub-

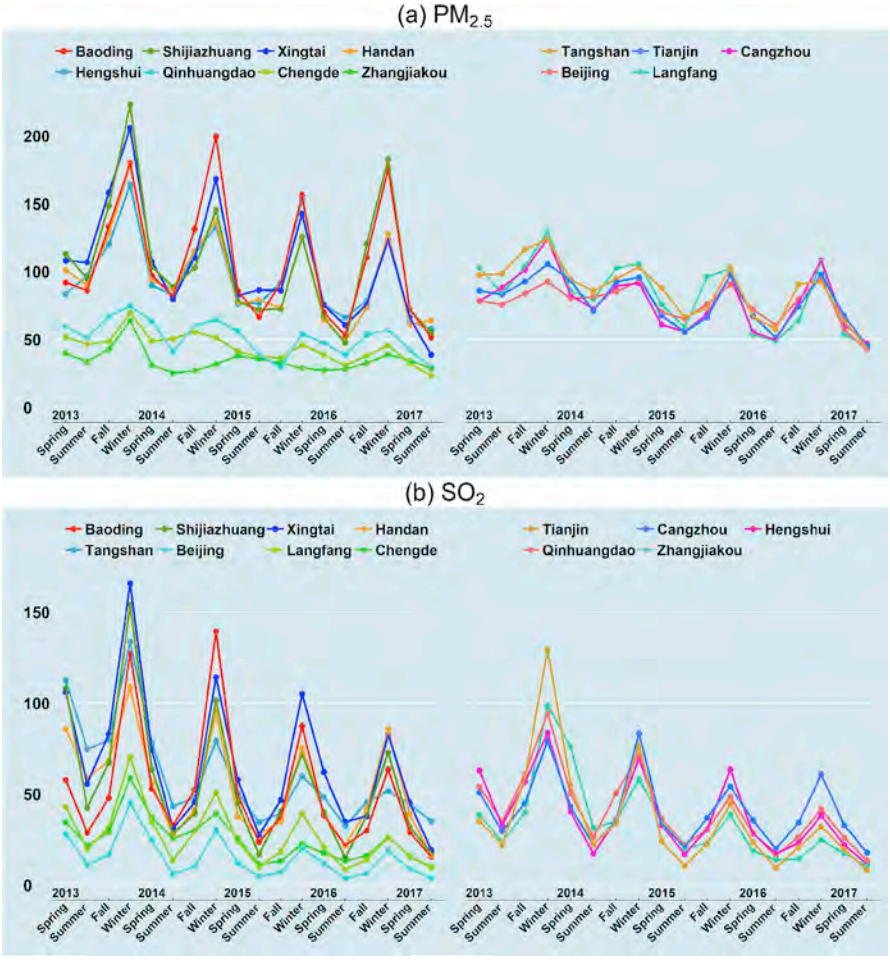

Fig. 7. Seasonal meteorologically adjusted averages of $PM_{2.5}$ and SO_2 concentrations (in $\mu g/m^3$) from spring 2013 to summer 2017 in BTH region.

Table 2
Cities in each three sub-regions for $PM_{2.5}$ and SO_2 based on the patterns of seasonal average concentrations.

Sub-region	$PM_{2.5}$	SO_2
Along Taihang	Baoding, Shijiazhuang, Xingtai, Handan, Hengshui	Baoding, Shijiazhuang, Xingtai, Handan, Tangshan
Bo Sea	Tangshan, Tianjin, Cangzhou, Beijing, Langfang	Cangzhou, Tianjin, Hengshui, Qinhuangdao
Northern	Zhangjiakou, Chengde, Qinhuangdao	Zhangjiakou, Chengde, Beijing, Langfanng

region endured the severest $PM_{2.5}$ pollution because of the high emissions by intensively heavy industrial installations as well as the Taihang mountain effect that creates less dispersive condition. The regionalization for SO_2 was a little different from that of $PM_{2.5}$ as shown in Table 2. The major change is the steel capital of the world Tangshan that joins Along Taihang sub-region due to its excessive SO_2 from the large scale steel making operation all year around.

Another different feature between $PM_{2.5}$ and SO_2 is the seasonal variation that SO_2 is larger than that of $PM_{2.5}$ as represented by the winter to summer concentration ratios. Cities such as Shijiazhuang, Handan, Baoding, Beijing and Tianjin have the ratios being around 4. A reason for the much higher winter to summer ratio is the winter heating which burns much coal and generate excessive SO_2. In cities such as Tangshan whose seasonal variation is much milder with the winter to summer ratio ranging only between 1.5 and 2, which is consistent to the fact that coal-burning is an all year affair for steel and iron production in Tangshan.

Fig. 8 reports the raw seasonal average of $PM_{2.5}$ which is an un-adjusted counterpart of Fig. 7 for $PM_{2.5}$. By comparing Figs. 7 and 8, the most noticeable difference between the adjusted and the un-adjusted raw averages is the elevated adjusted averages for the winter of 2016. The raw averages suggested a continued downward trend in the winter of 2016 in the $PM_{2.5}$ especially in the Along Taihang sub-region. However, the adjusted concentrations indicate the pollution situation in the winter of 2016 was actually worse than the winter 2015 if compared under the baseline meteorological conditions. This can be easily seen from Fig. 9(a) which shows that for Baoding, Handan, Cangzhou, Langfang and Qinhuangdao, the raw winter averages decreased from 2015 to 2016, while the adjusted averages indicated an increasing instead. This was consistent to a rebound in winter 2016 compared to 2015 in Hebei of the coal consumption for metal and steel production that increased from 2583.3 to 2644.18 (in unit ten thousand tons) and from 4486 to 4585 (in unit ten thousand tons) respectively, as shown in Figs. S10–S11 in the SM. These add more to the need for using the adjusted averages in additional to what we have presented in Section 4.1.

From Fig. 9, it is observed that the differences between the raw and adjusted averages were much larger in winter than the other seasons for both $PM_{2.5}$ and SO_2. The average of the absolute differences for $PM_{2.5}$ was 20 $\mu g/m^3$ in winter while those for the other three seasons were less than 5 $\mu g/m^3$, which indicated the influence of meteorological conditions in winter was much larger than the other seasons. This was the case especially for cities near the Taihang mountain like Baoding, Shijiazhuang, Xingtai and Handan that are larger than 26 $\mu g/m^3$.

Despite the rise in the winter concentration of 2016 in some cities, there were obvious declines in $PM_{2.5}$ and SO_2 levels in the BTH region

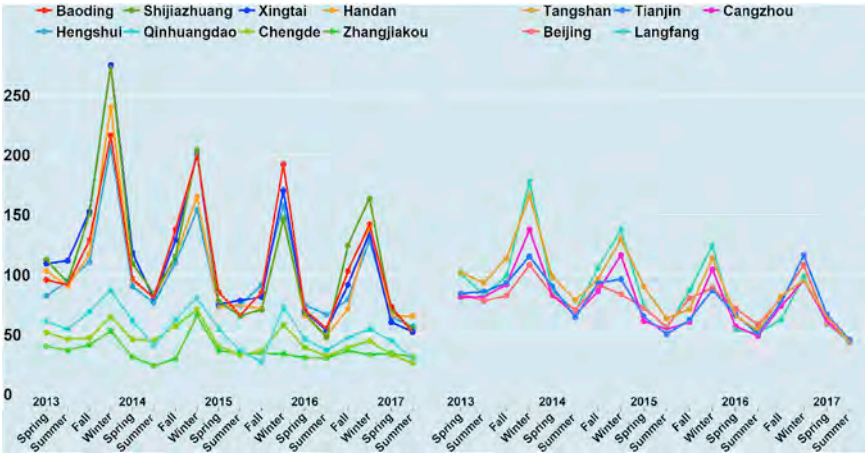

Fig. 8. Seasonal raw average time series of $PM_{2.5}$ (in $\mu g/m^3$) for the 13 cities in BTH region.

in a longer temporal time-span as easily found in Figs. 9 and 7. Fig. 10 displays the cumulative reduction percentages in the annual adjusted averages over the four seasonal years from 2013 to 2016. It shows that 9 out of the 13 cities had attained the 25% reduction target on $PM_{2.5}$ which is required by "National Ten Point Plan". On average, the adjusted $PM_{2.5}$ concentrations had dropped from 100.1 $\mu g/m^3$ in 2013 to 72.5 $\mu g/m^3$ in 2016, representing a 27% reduction. We also note that despite the declines in $PM_{2.5}$, the $PM_{2.5}$ levels are still above the international standards, which is 35 $\mu g/m^3$ by the US EPA or 20 $\mu g/m^3$ by the European Union.

The most striking aspect of the BTH regional air-quality data was a profound decline in SO_2. The regional average of SO_2 had dropped from 63.6 $\mu g/m^3$ in 2013 to 31.1 $\mu g/m^3$ in 2016, representing a 51% reduction. The substantial decline in SO_2 shows the significant achievement in reducing the consumption of the coal by several initiatives. These initiatives include the elimination of high energy consumption and high polluting equipments, efforts to phase out coal with the natural gas in power generation and winter heating in major cities, and to

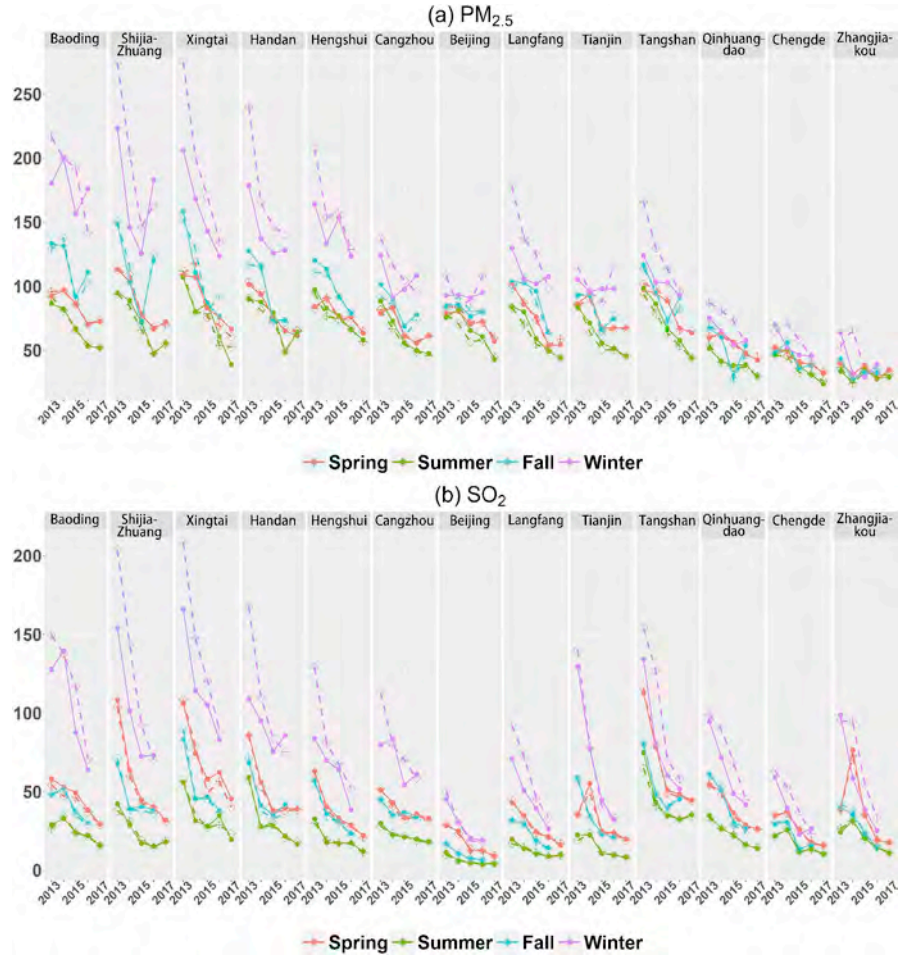

Fig. 9. Seasonal raw averages (dashed line) and meteorologically adjusted averages (solid line) time series of $PM_{2.5}$ and SO_2 (in $\mu g/m^3$) from spring 2013 to summer 2017 for the 13 cities in BTH region.

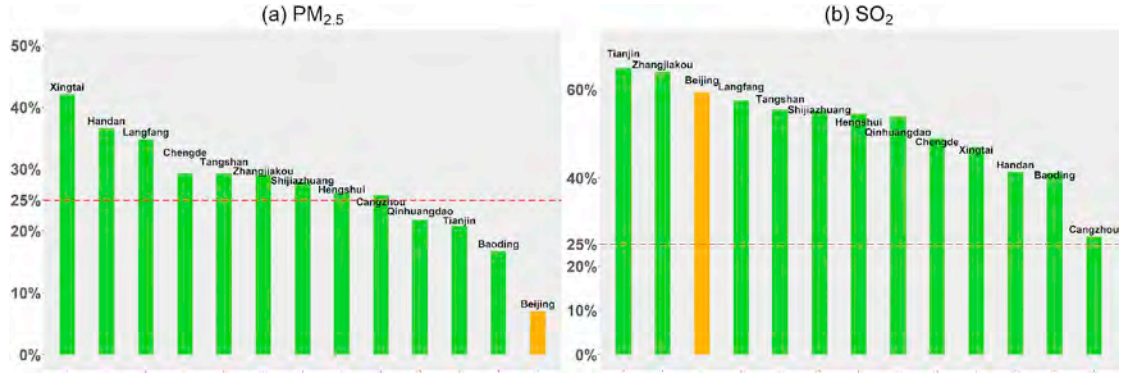

Fig. 10. Cumulative percentages of reduction in the annually adjusted averages of $PM_{2.5}$ and SO_2 concentrations from 2013 to 2016 in the 13 cities in BTH region.

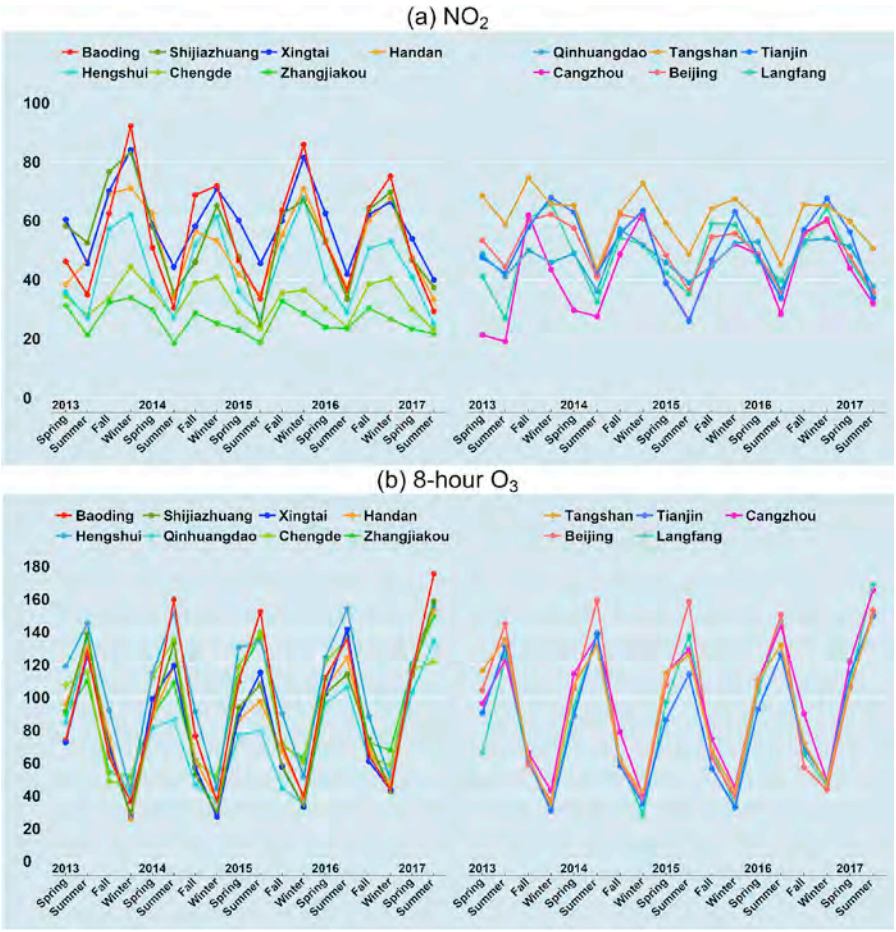

Fig. 11. Seasonal meteorologically adjusted averages of NO_2 and O_3 (in $\mu g/m^3$) from spring 2013 to summer 2017.

increase the usage of the natural gas and electricity in the rural domestic cooking and winter heating. These are reflected by a 20.7% declining in the consumption of coals in BTH from 387 million tons in 2013 to 307 million tons in 2016 as shown in Figs. S7–S10 of SM.

However, the decline in SO_2 had not translated to a significant reduction in $PM_{2.5}$ for some cities in BTH, indicating the complexity of PM generation process and the important roles of other precursors played in the process.

5.2. NO_2 and O_3

Nitrogen dioxide (NO_2) is a common air pollutant and also a precursor to nitrates and the ground level O_3. Under the strong sunlight, NO_2 reacts with oxygen in the air, producing another air pollutant, ozone (Toro et al., 2006). Different from the stratospheric ozone that protects humans from ultraviolet radiation, ground ozone causes harm to human respiratory and nervous system.

We applied the same adjustment method to the NO_2 and the 8-h (from 12pm to 7pm) ozone data, and calculated their seasonal adjusted averages which are shown in Fig. 11. In the adjustment of the 8-h ozone, we use the logarithm of the cumulative UVB to replace PRES as the correlation between PRES and the O_3 levels is small. It is seen from Fig. 11 that NO_2 follows a similar seasonal pattern to $PM_{2.5}$ and SO_2 in that the concentrations are the highest in winter and the lowest in summer. The seasonal pattern for O_3 is opposite that the highest levels occurs in summer and spring and the lowest in winter, which is

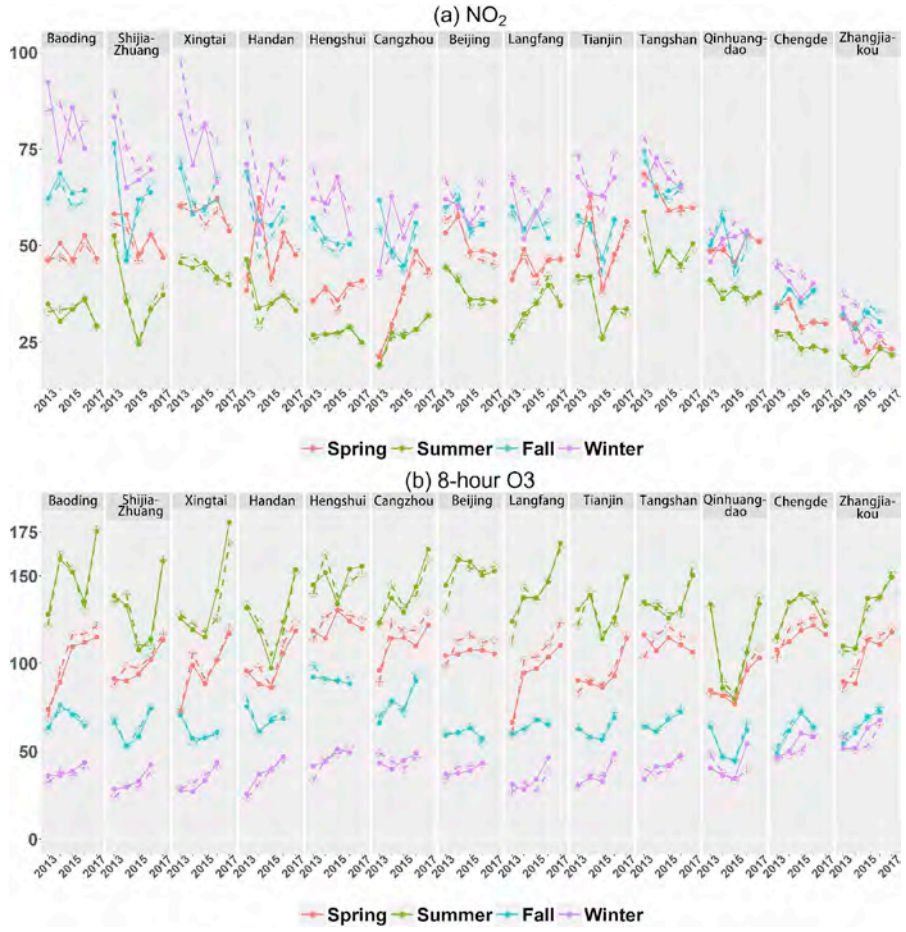

Fig. 12. Seasonal raw averages (dashed line) and meteorologically adjusted averages (solid line) time series of NO_2 and 8-h O_3 (in $\mu g/m^3$) from spring 2013 to summer 2017 for the 13 cities in BTH region.

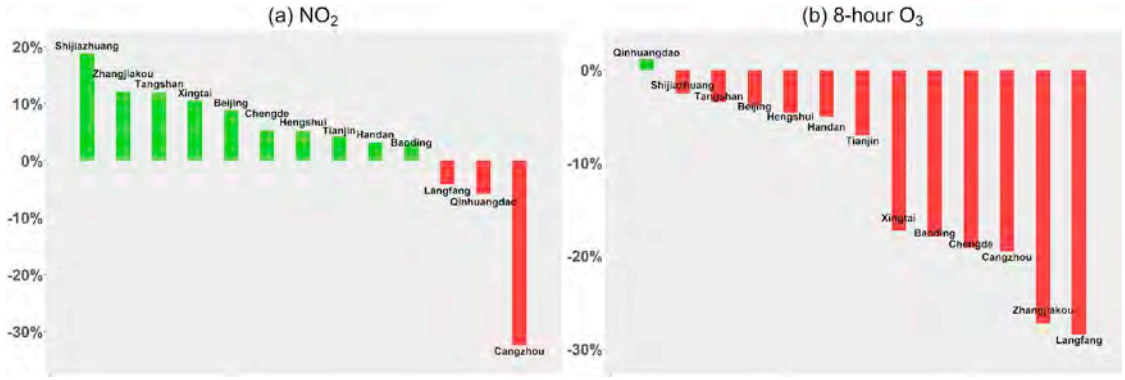

Fig. 13. Cumulative percentages of reduction in the annually adjusted averages of NO_2 and 8-h O_3 concentrations from 2013 to 2016 in the 13 cities in BTH region.

consistent to the annual intensity cycle of the ultraviolet radiation from the sun. The O_3 level in the summer could be 5 times of the winter level in some cities. However, for both NO_2 and O_3, the significant regional segmentation observed in $PM_{2.5}$ and SO_2 become less distinct for NO_2 and completely disappears for O_3.

Fig. 12 reports the time series of the raw and adjusted average concentrations for both pollutants in each season, allowing a better view of the trend without seasonal interference. Similar to $PM_{2.5}$ and SO_2, the difference between the unadjusted and adjusted seasonal average concentration for NO_2 is largest in winter, showing the impact of the meteorological condition. But for O_3, it shows that larger differences between the unadjusted and the adjusted 8-h O_3 concentrations happened in the spring when it tended to have larger variations among the key meteorological variables that affect the ozone level.

Fig. 13 presents the cumulative four years' changes in the adjusted average concentrations. It is observed that the NO_2 concentrations in a majority of the cities in BTH had decreased, but at much smaller rates compared to those of $PM_{2.5}$ and SO_2. The annual average NO_2 concentrations of BTH only declined by a mere 4.5% over the four years. But NO_2 concentrations in the three cities (Langfang, Qinhuangdao and Cangzhou) had increased, and Cangzhou increased the most by 32.4% over the four years.

The situation for the 8-h O_3 is a different scene: a steady regional-wide increase in the past four years. The annual average of 8-h O_3 concentrations in BTH had increased from 81.1 $\mu g/m^3$ in 2013 to 90.3 $\mu g/m^3$ in 2016, representing a 11.3% increase. If we focus on the 8-h O_3

in the spring and summer, the situation becomes even more alarming. For spring, BTH's average had increased from 93.0 $\mu g/m^3$ in 2013 to 113.9 $\mu g/m^3$ in 2017, a 22.5% rise that is larger than the increase in the annual average. The regional 8-h O_3 average in summer had already reached 129.8$\mu g/m^3$ in 2013, exceeding the 100$\mu g/m^3$ threshold level specified in the national standard. By the summer of 2017, it had increased to 155.0 $\mu g/m^3$, representing a 19.4% increase over the 2013's level.

The worsening O_3 situation in BTH is also reflected in the 90% quantiles of 8-h concentration of O_3 in summer given in the SM. Indeed, the average of the 13 cities' 90-percentile of 8-h O_3 had increased from 208.1 $\mu g/m^3$ in 2013 to 233.7 $\mu g/m^3$ in 2017, rising by 12.1%. Beijing endures the highest 90% quantile concentration in BTH in the last five summers, and reached 270.5 $\mu g/m^3$ in 2017.

It is clear that the ground ozone concentration has worsened significantly in the last four and half years, except Qinhuangdao with a small 1.2% improvement. Ozone has taken over the $PM_{2.5}$ as the primary pollutant in summer and spring. NO_x and the volatile organic components (VOC) constitute are known to be the important precursors of the ground ozone generation (Toro et al., 2006). However, components of VOC are not measured by the national air quality monitoring network. The very limited reduction in NO_2 over BTH means that there had been sustained supply of the precursors for O_3 generation. Although NO_2 had not increased, the regional-wide reduction in the PMs had increased the intensity of the ultraviolet radiation, which makes the oxidization of NO_2 for O_3 generation more efficient, indicating a negative effect of improving PM situation on O_3. This is inevitable if the NO_2 and its precursors are left to be un-managed, which has been the case for BTH as reflected by the sluggish results of NO_2.

6. Conclusion

The raw observed concentrations of pollutants are highly affected by the meteorological conditions, which makes the comparison between raw averages face the confounding problem. Our study adopts a meteorological method that could remove the meteorological confounding and calculates the seasonal adjusted mean for $PM_{2.5}$, SO_2, NO_2 and O_3 from spring in 2013 to summer in 2017. Our study finds significant declines in the particulate matters and sulfur dioxide in BTH. It also reveals a significant increase in the ground ozone level at alarming rates and a static nitrogen dioxide concentration over the last four years. These indicate the air quality management in BTH should be transformed from a sole target of $PM_{2.5}$ to a new system with dual targets of $PM_{2.5}$ and O_3. This new dual target system should have the list of the primary precursors extended to include NO_x and volatile organic compounds which demand new steps in the next phase of air quality management for BTH.

Acknowledgment

This research is funded by China's National Key Research Special Program Grant 2016YFC0207701 and 2016YFC0207702, National Key Basic Research Program Grant 2015CB856000 and National Natural Science Foundation of China grants 71532001, 71371016 and 11601356.

Appendix A. Supplementary data

Supplementary data related to this article can be found at https://doi.org/10.1016/j.atmosenv.2018.08.047.

References

Baccarelli, A.A., Zheng, Y., Zhang, X., Chang, D., Liu, L., Wolf, K.R., Zhang, Z., Mccracken, J.P., Díaz, A., Bertazzi, P.A., 2014. Air pollution exposure and lung function in highly exposed subjects in Beijing, China: a repeated-measure study. Part. Fibre Toxicol. 11, 51.

Baker, K., Scheff, P., 2007. Photochemical model performance for $PM_{2.5}$ sulfate, nitrate, ammonium, and precursor species SO_2, HNO_3, and NH_3 at background monitor locations in the central and eastern United States. Atmos. Environ. 41, 6185–6195. URL: http://www.sciencedirect.com/science/article/pii/S1352231007003330. https://doi.org/10.1016/j.atmosenv.2007.04.006.

Chen, S.X., Tang, C.Y., 2008. Nonparametric inference of value-at-risk for dependent financial returns. J. Financ. Econom. 3, 227–255.

Chen, Y., Ebenstein, A., Greenstone, M., Li, H., 2013. Evidence on the impact of sustained exposure to air pollution on life expectancy from China's Huai River policy. Proc. Natl. Acad. Sci. Unit. States Am. 110, 12936–12941. https://doi.org/10.1073/pnas.1300018110. URL: http://www.pnas.org/content/110/32/12936.abstract.

Chen, Z., Zhang, T., Zhang, R., Zhu, Z., Ou, C., Guo, Y., 2017. Estimating $PM_{2.5}$ concentrations based on non-linear exposure-lag-response associations with aerosol optical depth and meteorological measures. Atmos. Environ. 173, 30–37. URL: http://www.sciencedirect.com/science/article/pii/S135223101730729X. https://doi.org/10.1016/j.atmosenv.2017.10.055.

China's State Council, 2013. The Action Plan for Air Pollution Prevention and Control. URL: http://www.gov.cn/zwgk/2013-09/12/content_2486773.htm (in Chinese).

Dominici, F., Greenstone, M., Sunstein, C.R., 2014. Particulate matter matters. Science 344, 257–259.

Fan, J., Yao, Q., 2003. Nonlinear Time Series: Nonparametric and Parametric Methods. NY Springer.

Geng, G., Zhang, Q., Martin, R.V., van Donkelaar, A., Huo, H., Che, H., Lin, J., He, K., 2015. Estimating long-term $PM_{2.5}$ concentrations in China using satellite-based aerosol optical depth and a chemical transport model. Rem. Sens. Environ. 166, 262–270.

Guo, Y., Zeng, H., Zheng, R., Li, S., Barnett, A.G., Zhang, S., Zou, X., Huxley, R., Chen, W., Williams, G., 2015. The association between lung cancer incidence and ambient air pollution in China: a spatiotemporal analysis. Environ. Res. 144, 60–65.

Härdle, W., 1992. Applied Nonparametric Regression. Cambridge University Press.

Kampa, M., Castanas, E., 2008. Human health effects of air pollution. Environ. Pollut. 151, 362–367. URL: http://www.sciencedirect.com/science/article/pii/S0269749107002849. https://doi.org/10.1016/j.envpol.2007.06.012 Proceedings of the 4th International Workshop on Biomonitoring of Atmospheric Pollution (With Emphasis on Trace Elements).

Liang, X., Li, S., Zhang, S.Y., Huang, H., Chen, S.X., 2016. $PM_{2.5}$ data reliability, consistency, and air quality assessment in five Chinese cities. Journal of Geophysical Research-Atmospheres 121, 10220–10236. https://doi.org/10.1002/2016jd024877. < GotoISI > ://WOS:000384823000005.

Liang, X., Zou, T., Guo, B., Li, S., Zhang, H., Zhang, S., Huang, H., Chen, S.X., 2015. Assessing beijing's $PM_{2.5}$ pollution: severity, weather impact, APEC and winter heating. Proceedings of the Royal Society of London A: Mathematical, Physical and Engineering Sciences 471https://doi.org/10.1098/rspa.2015.0257. URL. http://rspa.royalsocietypublishing.org/content/471/2182/20150257.

Liu, L., Wang, Y., Du, S., Zhang, W., Hou, L., Vedal, S., Han, B., Yang, W., Chen, M., Bai, Z., 2016. Characteristics of atmospheric single particles during haze periods in a typical urban area of Beijing: a case study in October, 2014. J. Environ. Sci. 40, 145–153.

Liu, Y., Paciorek, C.J., Koutrakis, P., 2009. Estimating regional spatial and temporal variability of $PM_{2.5}$ concentrations using satellite data, meteorology, and land use information. Environ. Health Perspect. 117, 886.

Martin, R.V., 2008. Satellite remote sensing of surface air quality. Atmos. Environ. 42, 7823–7843.

Morgan, S.L., Winship, C., 2014. Counterfactuals and causal inference: models and principles for social research. Analytical Methods for Social Research, second ed. Cambridge University Press.

Pope, C.A., Burnett, R.T., Thun, M.J., Calle, E.E., Krewski, D., Ito, K., Thurston, G.D., 2002. Lung cancer, cardiopulmonary mortality, and long-term exposure to fine particulate air pollution. J. Am. Med. Assoc. 287, 1132–1141. https://doi.org/10.1001/jama.287.9.1132. < GotoISI > ://WOS:000174186000028.

Rich, D.Q., Liu, K., Zhang, J., Thurston, S.W., Stevens, T.P., Pan, Y., Kane, C., Weinberger, B., Ohman-Strickland, P., Woodruff, T.J., 2015. Differences in birth weight associated with the 2008 Beijing olympics air pollution reduction: results from a natural experiment. Environ. Health Perspect. 123, 880–887.

Tao, M., Chen, L., Li, R., Wang, L., Wang, J., Wang, Z., Tang, G., Tao, J., 2016. Spatial oscillation of the particle pollution in eastern China during winter: implications for regional air quality and climate. Atmos. Environ. 144, 100–110. URL: http://www.sciencedirect.com/science/article/pii/S1352231016306422. https://doi.org/10.1016/j.atmosenv.2016.08.049.

Toro, M.V., Cremades, L.V., Calbó, J., 2006. Relationship between VOC and NOx emissions and chemical production of tropospheric ozone in the Aburra Valley (Colombia). Chemosphere 65, 881.

Van Donkelaar, A., Martin, R.V., Brauer, M., Boys, B.L., 2015. Use of satellite observations for long-term exposure assessment of global concentrations of fine particulate matter. Environ. Health Perspect. 123, 135.

Wang, J., Xu, X., Spurr, R., Wang, Y., Drury, E., 2010. Improved algorithm for MODIS satellite retrievals of aerosol optical thickness over land in dusty atmosphere: implications for air quality monitoring in China. Rem. Sens. Environ. 114, 2575–2583.

Wang, L., Zhang, N., Liu, Z., Sun, Y., Ji, D., Wang, Y., 2014. The influence of climate factors, meteorological conditions, and boundary-layer structure on severe haze pollution in the Beijing-Tianjin-Hebei region during January 2013. Advances in Meteorology 2014, 14. https://doi.org/10.1155/2014/685971. URL: https://doi.org/10.1155/2014/685971.

Wang, Y., Zhuang, G., Xu, C., An, Z., 2007. The air pollution caused by the burning of fireworks during the lantern festival in Beijing. Atmos. Environ. 41, 417–431.

Yang, F., Tan, J., Zhao, Q., Du, Z., He, K., Ma, Y., Duan, F., Chen, G., Zhao, Q., 2011. Characteristics of $PM_{2.5}$ speciation in representative megacities and across China. Atmos. Chem. Phys. 11, 5207–5219. https://doi.org/10.5194/acp-11-5207-2011. URL: https://www.atmos-chem-phys.net/11/5207/2011/.